Optimized split-step method for modeling nonlinear pulse propagation in fiber Bragg gratings

Zeev Toroker* and Moshe Horowitz

Department of Electrical Engineering, Technion—Israel Institute of Technology, Haifa 32000, Israel
**Corresponding author: ztoroker@tx.technion.ac.il*

Received September 26, 2007; revised December 24, 2007; accepted January 7, 2008;
posted January 22, 2008 (Doc. ID 87686); published February 29, 2008

We present an optimized split-step method for solving nonlinear coupled-mode equations that model wave propagation in nonlinear fiber Bragg gratings. By separately controlling the spatial and the temporal step size of the solution, we could significantly decrease the run time duration without significantly affecting the result accuracy. The accuracy of the method and the dependence of the error on the algorithm parameters are studied in several examples. Physical considerations are given to determine the required resolution. © 2008 Optical Society of America

OCIS codes: 000.4430, 050.2770, 060.3735, 060.4370, 060.5530.

1. INTRODUCTION

Nonlinear effects and soliton propagation in fiber Bragg gratings (FBGs) have been extensively studied theoretically and experimentally [1–14]. Solitonic effects in such systems can be used for obtaining pulse compression [1,2], optical switching [3], optical AND gates [4–6], and for demonstrating the propagation of solitons with a slow group velocity [7,8]. To improve the performance of devices that are based on FBGs, there is a need to design and to optimize the grating structure. Nonlinear coupled-mode equations (NLCME) are used to model pulse propagation in nonlinear FBGs [9,12]. Two main numerical methods have been used to solve NLCME. The first is based on a numerical integration using implicit fourth-order method Runge–Kutta (RK) [13] and the second is based on using the split-step method [14]. The RK and split-step methods give results of similar accuracy when applied to the propagation of a single soliton. However, the computational run time of the split-step method is shorter by a factor of 20. However, even when the split-step method is used for designing gratings, the run time may remain of the order of several hours. Therefore, the performance optimization of nonlinear devices based on FBGs is limited.

In previous works, with both the RK integration and the split-step methods, a discrete solution of the NLCME with a temporal step size ΔT and a spatial step size ΔZ is used to represent the field envelope. The spatial and temporal step sizes are related by the group velocity V_g of the pulses in the absence of the grating by the equation $\Delta Z = V_g \Delta T$.

In this paper, we present an optimized split-step method (OSSM) for solving the NLCME numerically. An OSSM is a split-step method that does not require a direct relationship between temporal and spatial step sizes. The split-step method requires that a nonlinear and linear operator be solved separately in each iteration. We have found a generalized solution of the nonlinear operator and we use this solution in the OSSM. We have discovered that, with this new generalized solution, the spatial step size can be increased substantially without significantly affecting the accuracy of results. Hence, when applied to some important problems, the run time can be reduced by up to a hundredfold.

The spatial step size can be changed dynamically along the grating when using OSSM. When studying soliton launching, we could increase the spatial step-size beyond $V_g \Delta T$ by a factor of up to 100 in the uniform part of the grating. This also significantly reduced the run time in this region by a factor of up to ~100. Noticeably, there was no significant decrease in the accuracy of the solution. In highly nonuniform grating regions the spatial resolution should be of the same order as $\Delta Z = V_g \Delta T$. The overall run time for studying the launching was decreased by a factor of ~3.4.

We have demonstrated the use of OSSM for modeling soliton propagation, two-soliton interaction, optical bistability, and gap-soliton launching in FBGs. The dependence of the error on the spatial and the temporal resolution was studied for a single soliton propagation. In this example, an increase in temporal step size increased error primarily in the location of the soliton. On the other hand, we found that the increase in the error in soliton speed was small. This is not contradictory, since even small errors in soliton speed will result in large errors in soliton location after a sufficiently long passage of time. We show that the Richardson extrapolation may be used to decrease the run time slightly. To eliminate errors due to waves that are backreflected by the grating, an absorptive boundary window should be used at the grating ends.

2. THEORY

The NLCME

$$\pm i\partial_z u_\pm + iV_g^{-1}\partial_t u_\pm + \kappa(z)u_\mp + \Gamma(|u_\pm|^2 + 2|u_\mp|^2)u_\pm + \delta(z)u_\pm = 0, \tag{1}$$

are used to model nonlinear pulse propagation in FBGs [11]. In Eq. (1), $u_\pm(z,t)$ represents the field envelope of the forward (+) and backward (–) propagating waves, V_g represents the group velocity in the absence of the grating, Γ is the nonlinear coefficient, $\kappa(z)$ is the grating coupling strength, and $\delta(z)$ is the detuning parameter [14].

The split-step method is based on separating the propagation operator into a linear and a nonlinear operator. Each operator has a simple solution. In each small section of the medium, the propagation is calculated for each of the operators separately. The error in the solution of the split-step method is mainly because the two operators do not commute and the solution of the nonlinear operator is approximated. The split-step method is used extensively for solving the nonlinear Schrödinger equation (NLS) [15,16].

To implement the split-step method for solving the NLCME, Eq. (1) is presented in the form

$$\partial_t \mathbf{w} = (\hat{D} + \hat{N})\mathbf{w}, \tag{2}$$

where

$$\hat{D}(z) = V_g\begin{pmatrix} i\delta(z) & i\kappa(z) \\ i\kappa(z) & i\delta(z) \end{pmatrix}, \tag{3}$$

$$\hat{N}(z,t) = V_g\begin{pmatrix} \partial_z + N_-(z,t) & 0 \\ 0 & -\partial_z + N_+(z,t) \end{pmatrix}, \tag{4}$$

$$N_\mp(z,t) = i\Gamma(|u_\mp|^2 + 2|u_\pm|^2), \tag{5}$$

$$\mathbf{w} = \begin{bmatrix} u_-(z,t) \\ u_+(z,t) \end{bmatrix}.$$

The operator $\hat{N}(z,t)$ represents the nonlinear propagation effect, and the operator $\hat{D}(z)$ represents the linear effect due to the grating. The propagation in Eq. (1) is performed in the time domain rather than in the spatial domain as is often performed when solving the NLS equation. The NLCME describes the propagation of two counterpropagating waves. Therefore, the boundary conditions in the spatial domain are usually given at the two opposite sides of the grating. Such boundary conditions often make necessary the use of an iterative solution in cases when the equations are solved in the spatial domain. Since the input wave is usually launched only from one side of the grating, it becomes easier to implement the solution to the NLCME in the time domain.

We implemented two types of OSSM: nonsymmetrized and symmetrized. The solution of the nonsymmetrized OSSM is given by

$$\mathbf{w}(z,t+\Delta T) \simeq e^{\Delta T\cdot\hat{D}} e^{\int_t^{t+\Delta T}\hat{N}dt'}\mathbf{w}(z,t). \tag{6}$$

In the NLS equation, the local error has a leading order term of $O[(\Delta T)^2]$ [16], where $O[(\Delta T)^2]$ means $(\Delta T)^2$ is bounded for sufficiently small temporal step size ΔT.

The solution of the operator $\hat{D}$ is given by

$$\exp(\Delta T\cdot\hat{D}) = e^{i\delta h}\begin{pmatrix} \cos[\kappa(z)h] & i\sin[\kappa(z)h] \\ i\sin[\kappa(z)h] & \cos[\kappa(z)h] \end{pmatrix}, \tag{7}$$

where $h = V_g\Delta T$. To obtain the solution to the operator $\hat{N}(z,t)$, we use the following transformation:

$$\tau_\pm = \frac{1}{2}(V_g t \pm z). \tag{8}$$

The nonlinear operator $\hat{N}(\tau_+,\tau_-)$ in the new coordinate system, (τ_+,τ_-), is given by

$$\hat{N}(\tau_+,\tau_-) = \begin{pmatrix} N_-(\tau_+,\tau_-) & 0 \\ 0 & N_+(\tau_+,\tau_-) \end{pmatrix}, \tag{9}$$

where $N_\mp(\tau_+,\tau_-)$ are the functions defined in Eq. (5) expressed using the coordinates (τ_+,τ_-). The solution of Eq. (9) is given by

$$\begin{aligned} u_-(\tau_+,\tau_-+h) &= e^{\int_{\tau_-}^{\tau_-+h} N_-(\tau_+,\tau'_-)d\tau'_-}u_-(\tau_+,\tau_-) \\ u_+(\tau_++h,\tau_-) &= e^{\int_{\tau_+}^{\tau_++h} N_+(\tau'_+,\tau_-)d\tau'_+}u_+(\tau_+,\tau_-) \end{aligned}. \tag{10}$$

The integration in Eq. (10) can be performed using the rectangular integral approximation

$$\int_{\tau_-}^{\tau_-+h} N_-(\tau_+,\tau'_-)d\tau'_- \simeq hN_-(\tau_+,\tau_-),$$

$$\int_{\tau_+}^{\tau_++h} N_+(\tau'_+,\tau_-)d\tau'_+ \simeq hN_+(\tau_+,\tau_-). \tag{11}$$

These integrals have a local second-order error. After transforming $N_\pm(\tau_+,\tau_-)$ back to the original coordinates (z,t), the solution of the nonlinear propagation is given by

$$u_\mp(z\mp h, t+\Delta T) = \exp[hN_\mp(z,t)]u_\mp(z,t). \tag{12}$$

Substituting Eqs. (7) and (12) into Eq. (6) yields the following solution of the nonsymmetrized OSSM:

$$\begin{aligned} u_-(z,t+\Delta T) &= e^{i\delta h}\{\cos(\kappa h)\exp[hN_-(z+h,t)]u_-(z+h,t) \\ &\quad + i\sin(\kappa h)\exp[hN_+(z-h,t)]u_+(z-h,t)\}, \\ u_+(z,t+\Delta T) &= e^{i\delta h}\{\cos(\kappa h)\exp[hN_+(z-h,t)]u_+(z-h,t) \\ &\quad + i\sin(\kappa h)\exp[hN_-(z+h,t)]u_-(z+h,t)\}. \end{aligned} \tag{13}$$

The solution of the symmetrized OSSM is given by

$$\mathbf{w}(z,t+\Delta T) \simeq e^{\Delta T\hat{D}/2} e^{\int_t^{t+\Delta T}\hat{N}dt'} e^{\Delta T\hat{D}/2}\mathbf{w}(z,t). \tag{14}$$

The local error in the case of NLS is of the order of $O[(\Delta T)^3]$ [15].

In the symmetrized OSSM, the solution of the operator $\hat{D}$ is given by Eq. (7) with $\Delta T/2$ substituted for ΔT. The solution of the nonlinear operator $\hat{N}(z,t)$ is given in Eq. (10). In the symmetrized OSSM, the integration in Eq. (10) is performed more accurately using the trapezoid integral approximation:

$$\int_{\tau_-}^{\tau_-+h} N_-(\tau_+,\tau'_-)\mathrm{d}\tau'_- \simeq \frac{1}{2}h[N_-(\tau_+,\tau_-)+N_-(\tau_+,\tau_-+h)],$$

$$\int_{\tau_+}^{\tau_++h} N_+(\tau'_+,\tau_-)\mathrm{d}\tau'_+ \simeq \frac{1}{2}h[N_+(\tau_+,\tau_-)+N_+(\tau_++h,\tau_-)]. \tag{15}$$

The trapezoid approximation has a local third-order error. Transforming the result back to the original coordinates (z,t) yields the solution of the nonlinear propagation:

$$u_\mp(z\mp h,t+\Delta T)=e^{(h/2)[N_\mp(z,t)+N_\mp(z\mp h,t+\Delta T)]}u_\mp(z,t). \tag{16}$$

The solution of the symmetrized OSSM is given by

$$\begin{aligned}u_-(z,t+\Delta T)=e^{i\delta h}\Bigg[&\cos(\kappa h)\exp\Bigg\{\frac{h}{2}[N_-(z+h,t)\\&+N_-(z,t+\Delta T)]\Bigg\}u_-(z+h,t)\\&+i\sin(\kappa h)\exp\Bigg\{\frac{h}{2}[N_+(z-h,t)\\&+N_+(z,t+\Delta T)]\Bigg\}u_+(z-h,t)\Bigg],\end{aligned}$$

$$\begin{aligned}u_+(z,t+\Delta T)=e^{i\delta h}\Bigg[&\cos(\kappa h)\exp\Bigg\{\frac{h}{2}[N_+(z-h,t)\\&+N_+(z,t+\Delta T)]\Bigg\}u_+(z-h,t)\\&+i\sin(\kappa h)\exp\Bigg\{\frac{h}{2}[N_-(z+h,t)\\&+N_-(z,t+\Delta T)]\Bigg\}u_-(z+h,t)\Bigg].\end{aligned} \tag{17}$$

The functions $N_\mp(z,t+\Delta T)$ are calculated using a two-step iterative procedure [16]. Initially, the functions $N_\mp(z,t+\Delta T)$ are replaced by $N_\mp(z,t)$ in Eq. (17). The results $u_\pm(z,t+\Delta T)$ are then used to calculate the new value of $N_\mp(z,t+\Delta T)$. We repeat this iteration two times to obtain an accurate enough result for $N_\mp(z,t+\Delta T)$.

In this paper, we have compared results of the nonsymmetrized OSSM with results of the symmetrized OSSM. We have found the nonsymmetrized OSSM as compared to the symmetrized OSSM to require less run time and to yield results of similar accuracy.

The nonsymmetrized OSSM in Eq. (13) and the symmetrized OSSM in Eq. (17) require spatial shifts of $\pm h=\pm V_g\Delta T$ in the location z. The shift operation originates in the coordinate transformation in Eq. (8). In the case of a spatial step size equal to $\Delta Z=V_g\Delta T$, the spatial shift is simply a shift of the discrete solutions $u_\pm(z,t)$ by one spatial step size either forward or backward as in [14]. For example, consider the discretized spatial axis $\{z_n\}_{n=1}^N$ with spatial step size $z_{n+1}-z_n=\Delta Z=V_g\Delta T$. For $n=1,2,\ldots,N$, a left spatial shift of the field envelopes $u_\pm(z_n,t)$ by h is given by

$$u_\pm(z_n+h,t)=\begin{cases}u_\pm(z_{n+1},t) & n=1,\ldots,N-1\\ 0 & n=N\end{cases}. \tag{18}$$

A right spatial shift of the field envelopes $u_\pm(z_n,t)$ by h is given by

$$u_\pm(z_n-h,t)=\begin{cases}0 & n=1\\ u_\pm(z_{n-1},t) & n=2,\ldots,N\end{cases}. \tag{19}$$

In the OSSM we allowed the spatial step size ΔZ to be different than h. In the case $h=N\Delta Z$ (where $N>1$ is an integer), the spatial shift operation in Eqs. (12) and (16) is simply performed by shifting the discrete solution of $u_\pm(z,t)$ by N times the spatial step size ΔZ. Depending on the direction of the shift, zeros should be added at the beginning or at the end of the solution. However, in case $(V_g\Delta T)<\Delta Z$, or the case that the ratio between h and ΔZ does not equal an integer, the spatial shift is performed using the Fourier transform,

$$u_\mp(z\pm h,t+\Delta T)=\mathrm{IFT}\{e^{\pm jkh}\mathrm{FT}[u_\mp(z,t)]\}, \tag{20}$$

where FT and IFT are the Fourier and the inverse Fourier transform, respectively, that are performed in the spatial domain, and k is the spatial frequency.

The step-size ΔZ can be dynamically changed during the pulse propagation in order to optimize performance. In the case $h=N\Delta Z$, some of the points in the array representing the discrete field should be simply deleted. However, when the spatial step size ΔZ should be decreased, the Shannon Sampling Theorem can be used to interpolate the missing points [17]:

$$u_\pm(z_m,t)=\sum_{n=1}^{M}u_\pm(z_n,t)\mathrm{sinc}[\omega_c(z_m-n\Delta z_o)], \tag{21}$$

where $z_n=(n-1)\Delta z_o$ is the old spatial grid, M is the number of points used to represent the discrete field in the old resolution, $z_m=(m-1)\Delta z$ is the new spatial grid with a spatial step size of $\Delta z<\Delta z_o$, and $\omega_c=\pi/\Delta z_o$.

The ability to control the spatial resolution along the pulse propagation results in a significant reduction in the run time of the numerical solution. We demonstrate this in Section 3. In regions of the grating in which there is not a fast change in the pulse, the spatial step size ΔZ can be chosen to be significantly larger than $V_g\Delta T$. For example, in the case of an interaction between two solitons, the spatial step size can be increased by a factor of 10 to $10V_g\Delta T$ without significantly affecting the accuracy of solutions. When launching a soliton, an apodization section is used in the grating entrance in order to decrease the pulse reflection. In the apodization region, the spatial step size ΔZ should be of the order of $V_g\Delta T$. On the other hand, in the uniform region of the grating, ΔZ can be of the order of $100V_g\Delta T$. Hence, the run time in this region can be decreased by a factor of $\sim$100.

3. NUMERICAL RESULTS

We will demonstrate the advantages of the OSSM in solving four different problems. In three of the problems, the length of the grating is infinite. These problems are the propagation of a soliton, the collision of two solitons, and the launching of a soliton. In our simulation, we used a spatial window with finite width L of the order of tens of centimeters.

In FBGs, the speed of solitons is sometimes significantly lower than the speed of dispersive waves that propagate in the grating. This is a physical phenomenon. Dispersive waves are sometimes generated during the interaction of solitons or when launching a soliton. However, in the simulation, when dispersive waves arrive at the boundaries of the window, they may be falsely modeled to be backreflected. Also, due to aliasing in the fast Fourier transform (FFT) operation in Eq. (20), dispersive waves may be falsely modeled to reenter the opposite side of the window. In case of infinite gratings, such waves should simply exit the spatial region in which solitons are concentrated. Therefore, dispersive waves may be simulated incorrectly.

The simplest way to overcome these problems is, at each propagation step, to multiply the fields by an absorbing window [18–20]. In our simulations we used this approach with a window function given by

$$W(z)=\begin{cases}\sin^{1/3}\left[\pi\left(z+\dfrac{L}{2}\right)\Big/(2L_a)\right] & -\dfrac{L}{2}\le z\le -\dfrac{L}{2}+L_a\\ 1 & -\dfrac{L}{2}+L_a\le z\le \dfrac{L}{2}-L_a\\ -\sin^{1/3}\left[\pi\left(z-\dfrac{L}{2}\right)\Big/(2L_a)\right] & \dfrac{L}{2}-L_a\le z\le \dfrac{L}{2}\end{cases}, \tag{22}$$

where L is the width of the window, and L_a is the width of each absorbing layer. The location of the grating region in which the fields are of interest is $-L_w/2\le z\le L_w/2$, where $L_w<(L-2L_a)$. In the following examples we required that $L-L_w\ge 10W_m$, where W_m is the maximum spatial full width at half-maximum (FWHM) of the propagating pulses' intensity.

Another method commonly used to overcome the boundary reflection problem is to add a perfectly matched layer (PML) [21]. This method has been applied recently in FBGs [22]. Although this method reduces the reflection effects, it requires the solution of an additional propagation equation in the matched layer. Hence, it is more computationally demanding.

A. Propagation of a Soliton

In the first example, we compared the split-step solution given in Eq. (6) to the known one-soliton solution that describes the propagation of a single soliton in an infinite uniform grating [9]. The coupling coefficient and the nonlinear coefficients of the grating were equal to $\kappa=9000\ \mathrm{m}^{-1}$ and $\Gamma=5\ \mathrm{km}^{-1}\,\mathrm{W}^{-1}$, respectively. The effective refractive index in the absence of the grating was equal to $n=1.45$. The soliton parameters, as defined in [11], were $(\tilde{\delta},v)=(0.02,0.12)$. The input soliton had a spatial FWHM of $W_S=9.72$ mm and a peak power of 478.8 W. The frequency offset relative to the Bragg frequency of the grating was equal to 298.46 GHz. We compare the result of the nonsymmetrized OSSM to the analytical one-soliton solution given in [9]. To simulate an infinite grating we used the window function of Eq. (22). The parameters were chosen as follows: $L=40$ cm, $L_w=30$ cm, and $L_a=2$ cm. We define the relative error between the analytical one-soliton solution $I_1(z,t)$ and the numerical solution $I_2(z,t)$ at time t by

$$\varepsilon=\frac{\|I_1-I_2\|}{\|I_1\|}, \tag{23}$$

where $\|I_i(z,t)\|=(\int|I_i(z,t)|^2\mathrm{d}z)^{1/2}$ $(i=1,2)$ and $I_i(z,t)=|u_{i,+}(z,t)|^2+|u_{i,-}(z,t)|^2$. Figure 1 compares the results obtained using nonsymmetrized OSSM with a spatial step size of $\Delta Z=V_g\Delta T$ (dashed–dotted curve) and ΔZ

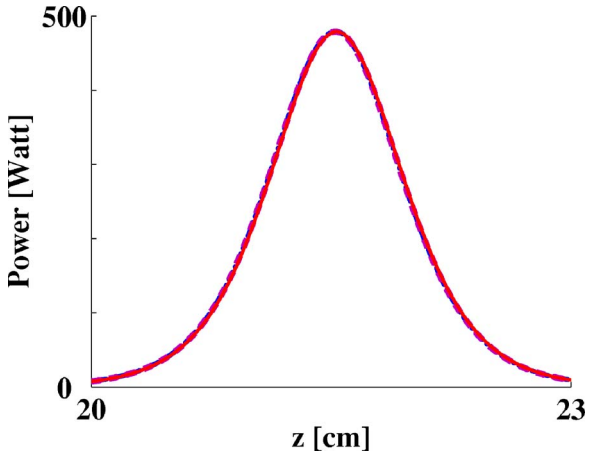

Fig. 1. (Color online) Comparison between the intensity calculated using the explicit one-soliton solution in FBGs [9] (solid curve) and the numerical solution obtained using nonsymmetrized OSSM with a spatial step size of $\Delta Z=W_S/40$ (dashed curve) and $\Delta Z=W_S/2400$ (dashed–dotted curve), where $W_S=9.72$ mm is the spatial FWHM of the soliton. The temporal step size was equal in both cases to $\Delta T=W_S/(2400V_g)$ and the result was calculated after the soliton propagated a distance of 13.5 cm inside the grating.

$=60V_g\Delta T$ (dashed curve).The temporal step size in both cases was equal to $\Delta T=W_S/(2400V_g)$, where W_S is the spatial FWHM of the soliton. The comparison was performed at $t=5.45$ ns, which corresponds to a propagation of the soliton through a distance of 13.5 cm inside the grating. The relative error was equal to 0.964% for a spatial step size of $\Delta Z=V_g\Delta T$ and 0.9641% for a spatial step size of $\Delta Z=60V_g\Delta T$. The increase of the spatial step size made it possible to decrease the run time from 6 h into only 8 min while keeping a similar accuracy.

Figure 2 compares the results obtained using different temporal step sizes of $\Delta T=W_S/(1600V_g)$, $W_S/(800V_g)$, $W_S/(4000V_g)$, and $W_S/(200V_g)$. The spatial step size in all cases was kept constant, $\Delta Z=W_S/40$. The comparison was performed after the soliton propagated through a distance of 13.5 cm inside the grating. The figure shows that as the temporal step size increases, the error in the soliton amplitude and in the soliton location increases. Figure 3 shows the global relative error as a function of the normalized temporal step size, $\Delta TV_g/W_S$, after the soliton has propagated through a distance of 13.5 cm inside the grating. The nonsymmetrized OSSM made it possible to keep in all the calculations a constant spatial step size of $\Delta Z=W_S/40$. The figure indicates that when the propagation of a single soliton is calculated, the relative error approximately depends on the square of the temporal step size. Therefore, the global error is of the order of $O[(\Delta T)^2]$ rather than an error of the order of $O[(\Delta T)]$ as one may expect, since we used the nonsymmetrized split-step method given in Eq. (6). A similar dependence of the error was also found in the next example, where a two-soliton interaction was studied.

We define the amplitude error or the relative error in the peak intensity at time t as

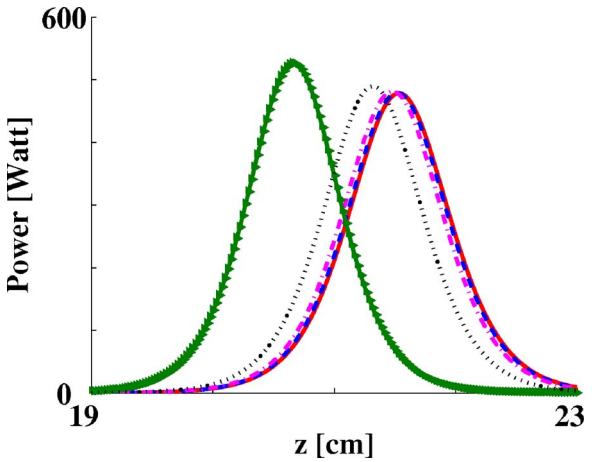

Fig. 2. (Color online) Comparison between the intensity of the explicit one-soliton solution (solid curve) and the numerical solution that was calculated using nonsymmetrized OSSM with a temporal step size of $\Delta T=W_S/(1600V_g)$ (dashed curve), $\Delta T=W_S/(800V_g)$ (dashed–dotted curve), $\Delta T=W_S/(4000V_g)$ (dotted curve), and $\Delta T=W_S/(200V_g)$ (left-pointing triangle marker). The comparison was performed after the soliton had propagated a distance of 13.5 cm along the grating. The spatial step size was equal to $\Delta Z=W_S/40$.

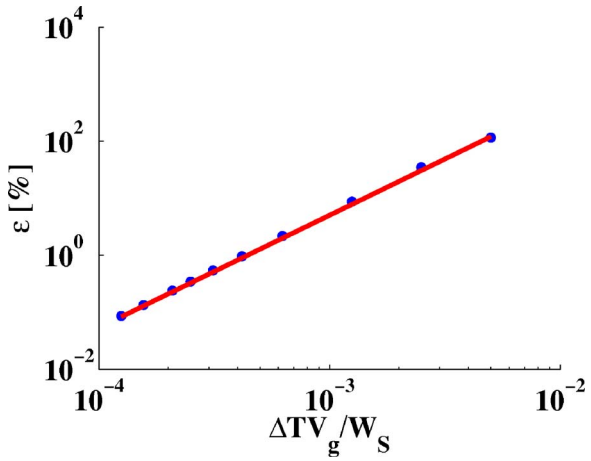

Fig. 3. (Color online) Relative error, defined in Eq. (23), between the explicit one-soliton solution and the numerical results as a function of the temporal step size, $\Delta TV_g/W_S$, calculated after the soliton has propagated a distance of 13.5 cm along the grating. The spatial step size was equal to $\Delta Z=W_S/40$, where W_S is the spatial FWHM of the soliton. The solid line is a least-square mean error linear fit: $\ln(\varepsilon)=1.9708\ln(\Delta TV_g/W_S)+15.228$.

$$\varepsilon_a=\frac{|P_1-P_2|}{P_1}, \tag{24}$$

where $P_i=\max_z\{I_i(z,t)\}$ $(i=1,2)$ is the maximum intensity at time t calculated using the explicit one-soliton solution $(i=1)$ [9] and by using the OSSM $(i=2)$. The results were compared at $t=5.45$ ns, where $P_1=478.8$ W. The relative error in the soliton location at $t=5.45$ ns is defined by

$$\varepsilon_z=\frac{|Z_1-Z_2|}{W_S}, \tag{25}$$

where $Z_i=\int_{-\infty}^{\infty}zI_i(z,t)\mathrm{d}z/\int_{-\infty}^{\infty}I_i(z,t)\mathrm{d}z$ $(i=1,2)$ is the first-order moment of the soliton position at $t=5.45$ ns, and Z_1 is the exact soliton location that is equal to 21.54 cm. The results obtained in Fig. 4 indicate that for a single soliton

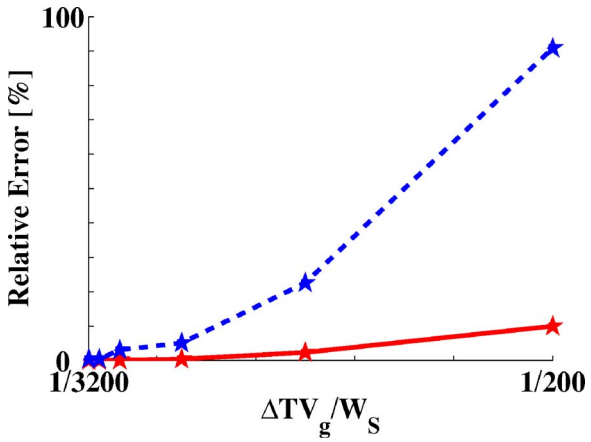

Fig. 4. (Color online) Relative error between the explicit one-soliton solution and the numerical results of the output soliton amplitude (solid curve) and the output soliton position (dashed curve) as a function of the temporal step size, ΔT, calculated after the soliton has propagated a distance of 13.5 cm along the grating. The spatial step size was equal to $\Delta Z=W_S/40$.

propagation, as the temporal step size decreases, the error in the soliton location converges more quickly than the error in its amplitude. A similar behavior of the error was obtained in all the examples analyzed in this work. The error in the speed of the soliton is defined by

$$\varepsilon_v = \frac{1}{vV_g}\frac{|\Delta Z(t_2) - \Delta Z(t_1)|}{t_2 - t_1}, \tag{26}$$

where $t_2 = 5.45$ ns, $t_1 = 2.63$ ns, $v = 0.12$, $\Delta Z(t) = Z(t) - Z_s(t)$, $Z(t)$ is the first-order moment of the soliton position at time t, and $Z_s(t)$ is the exact soliton location at time t. The relative errors in the speed were equal to 0.4%, 0.1%, and 0.004% for a temporal step size of $\Delta T = W_s/(800V_g)$, $\Delta T = W_s/(1600V_g)$, and $\Delta T = W_s/(8000V_g)$, respectively. The spatial step size was kept constant in all cases, $\Delta Z = W_s/40$. The results indicate that the error in the soliton speed is very small. However, this error is accumulated and it may cause an error in the soliton location, as can be observed in Fig. 4.

Since the small error in the soliton location usually does not have a significant physical meaning, one may increase the temporal step size and ignore the very small error in the soliton speed. However, the inaccuracy in the soliton location may significantly affect the error, as defined in Eq. (23).

The result shown in Fig. 1 indicated that, using the nonsymmetrized OSSM, we can increase the spatial step size ΔZ beyond $V_g\Delta T$ without a significant increase in the error. We have also checked the possibility of improving the result's accuracy by using the Richardson extrapolation [15,23]. This method was previously used to decrease the simulation run time when solving the NLS equation [15]. The Richardson extrapolation is based on propagating the solution in the time domain using a fine resolution ΔT and a coarse resolution $2\Delta T$.

Since the global error that was obtained in Fig. 3 was of the order of $O[(\Delta T)^2]$, we have implemented the Richardson extrapolation, assuming a local error of the order of $O[(\Delta T)^3]$. After performing the Richardson extrapolation, the local error is expected to be of the order of $O[(\Delta T)^4]$. We have verified that if we implement the Richardson extrapolation using coefficients that correspond to a local error of $O[(\Delta T)^2]$ or $O[\Delta T]$, the global error only increases compared to that obtained without using the extrapolation. Assuming a local error of the order of $O[(\Delta T)^3]$, the Richardson extrapolation is implemented using the connection [23]

$$u_{\pm}(z,t + 2\Delta T) = (8/7)u_{\pm}^{f}(z,t + 2\Delta T) - (1/7)u_{\pm}^{c}(z,t + 2\Delta T) + O[(\Delta T)^4], \tag{27}$$

where $u_{\pm}^{f}(z,t)$ and $u_{\pm}^{c}(z,t)$ are the solutions using the fine and the coarse resolution, respectively. By using the Richardson extrapolation with a fine temporal step size of $\Delta T = W_S/(6400V_g)$ and a spatial step size of $\Delta Z = W_S/40$, we obtained a relative error of 0.02% compared to an error of 0.13% that was obtained without using the Richardson extrapolation for a temporal step size of $\Delta T = W_S/(6400V_g)$. Therefore, the Richardson extrapolation improves the accuracy compared to that obtained using the fine resolution. However, the Richardson extrapolation also increased the run time to 18 min compared to a run time of 10 min that was obtained using the solution with the fine resolution. Similar results were obtained for a fine resolution of $W_S/(1600V_g)$ and for a spatial step size $\Delta Z = W_S/40$. The Richardson extrapolation enabled us in this case to reduce the error from 2.17% to 1.2%, while the run time increased from 7.5 to 11.5 min. We could also decrease the error to 0.96% without using the Richardson extrapolation by decreasing the temporal step size to $\Delta T = W_S/(2400V_g)$. The run time in this case was equal to 14 min. The results obtained indicate that the use of the Richardson extrapolation enables one to only slightly decrease the run time, while the use of the OSSM with a large spatial step size enables one to significantly decrease the run time without a significant increase in the result error, as shown in Fig. 1. We would also like to note that the Richardson extrapolation made it possible to increase the result's accuracy only when the fine temporal step size was lower than $\Delta T = W_S/(1600V_g)$.

B. Collision of Two Solitons

In the second example, we study the collision of two solitons in an infinite uniform grating with a coupling coefficient $\kappa = 9000\ \mathrm{m}^{-1}$. The nonlinear coefficient was equal to $\Gamma = 5\ \mathrm{km}^{-1}\ \mathrm{W}^{-1}$ and the effective refractive index in the absence of the grating was equal to $n = 1.45$. To simulate infinite grating, we used the window function of Eq. (22). The parameters were chosen as follows: $L = 105$ cm, $L_w = 85$ cm, and $L_a = 5$ cm. The soliton parameters, as defined in [11], were $(\tilde{\delta}_1, v_1) = (0.022, 0.1)$, $(\tilde{\delta}_2, v_2) = (0.02, 0.12)$. At $t = 0$, the spatial separation and the phase differences between the solitons' peaks were 6 cm and 0 rad, respectively. The input solitons had a spatial FWHM of 8.86 and 9.72 mm. The peak power of the two input solitons and their frequency offset relative to the Bragg frequency were equal to 582 W, 478.8 W, 297.78 GHz, and 298.46 GHz, respectively.

Figure 5 shows the interaction calculated using the

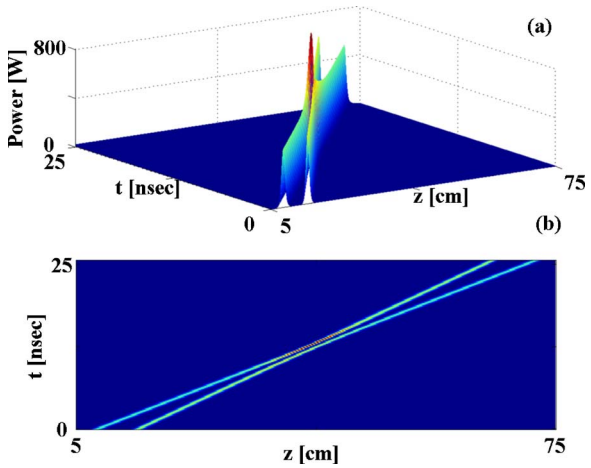

Fig. 5. (Color online) Collision between two solitons calculated using nonsymmetrized OSSM shown in (a) a three-dimensional plot and in (b) a two-dimensional plot. The simulation parameters were $\Delta Z = W_S/80$, $V_g\Delta T = W_S/800$, where $W_S = 8.86$ mm is the spatial FWHM of the shorter soliton. The peak power of the two input solitons and their frequency offset relative to the local Bragg frequency are equal to 582 W, 478.8 W, 297.78 GHz, and 298.46 GHz, respectively.

nonsymmetrized OSSM given in Eq. (13) for a spatial step size $\Delta Z = W_S/80$ and a temporal step size $\Delta T = W_S/800V_g$, where $W_S = 8.86$ mm is the spatial FWHM of the shorter soliton.

We have studied the convergence of the solution as a function of the temporal step size as performed in the previous example. Figure 6 compares the output intensity obtained at the end of the interaction at $t = 25.52$ ns using different temporal step sizes of $\Delta T = W_S/(8000V_g)$ (solid curve), $\Delta T = W_S/(1600V_g)$ (dashed–dotted curve), and $\Delta T = W_S/(800V_g)$ (dashed curve), where $W_S = 8.86$ mm is the input spatial FWHM width of the shorter soliton. The spatial step size was equal in all the calculations to $\Delta Z = W_S/40$. The figure indicates that when the temporal step size is equal to $\Delta T = W_S/(800V_g)$, the error is mainly caused due to a slight shift in the soliton locations. The run time in this case is equal to 1 h compared to a run time of 10 h using a temporal step size of $\Delta T = W_S/(8000V_g)$. Since the small shift in the solitons location usually does not have a physical significance one may use the larger temporal step size in order to decrease the run time.

Figure 7 compares the intensity of the two solitons after the interaction calculated using the nonsymmetrized OSSM given in Eq. (13) (dashed curve) with the results of the symmetrized OSSM given in Eq. (17) (solid curve). The spatial and the temporal step sizes were equal to $\Delta Z = W_S/800$ and $\Delta T = W_S/(800V_g)$, respectively. At the end of the interaction at $t = 25.52$ ns, the relative error between the results was equal only to $\epsilon = 0.007\%$. Thus, we ascertained that the relative error between the nonsymmetrized OSSM and the symmetrized OSSM is very small. This result was also verified for all the other examples given in this manuscript. Since the relative error between the two implementations is very low, we used the nonsymmetrized OSSM throughout the manuscript.

The nonsymmetrized OSSM makes it possible to increase the spatial step size and hence to significantly reduce the run time without a significant increase in error. To verify that the spatial step size ΔZ may be significantly increased compared to $V_g\Delta T$ without a significant increase in the error, we have analyzed the soliton interaction using a spatial step size $\Delta Z = 10V_g\Delta T$. The temporal step size $\Delta T = W_S/(800V_g)$ was the same as that used in Fig. 7. Figure 8 compares the pulse intensity obtained using the higher spatial step size, $\Delta Z = 10Vg\Delta T$ (solid curve), to that obtained using the lower spatial step size, $\Delta Z = Vg\Delta T$ (dashed curve). The relative error at the end of the interaction at $t = 25.52$ ns was equal to $\epsilon = 0.49\%$. By increasing the spatial step size ΔZ by a factor of 10, the run time decreased from 12 to 2 h without a significant increase in the error. The main reason that the time reduction that was obtained is less than the ratio between the two step sizes is that in the case when $\Delta Z \neq Vg\Delta T$, the spatial shift operation is implemented using FFT instead of just shifting an array and adding zeros.

We calculated the average speed of each soliton after the interaction as a function of the temporal step size. The average speed is defined as $\langle v_i \rangle = [Z_i(t_2) - Z_i(t_1)]/(t_2 - t_1)$, where $i = 1, 2$, $t_1 = 22.1$ ns, $t_2 = 25.5$ ns, $Z_i(t_1)$ is the lo-

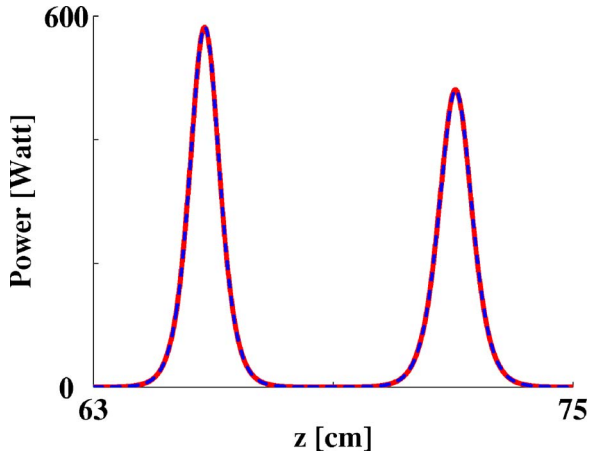

Fig. 7. (Color online) Intensity of two solitons, calculated at the end of their interaction at $t = 25.52$ ns, by using symmetrized OSSM (solid curve) and by using nonsymmetrized OSSM (dashed curve). The spatial and temporal resolution are $\Delta Z = W_S/800$ and $\Delta T = W_S/(800V_g)$, respectively. The solitons' parameters are the same as in Fig. 5.

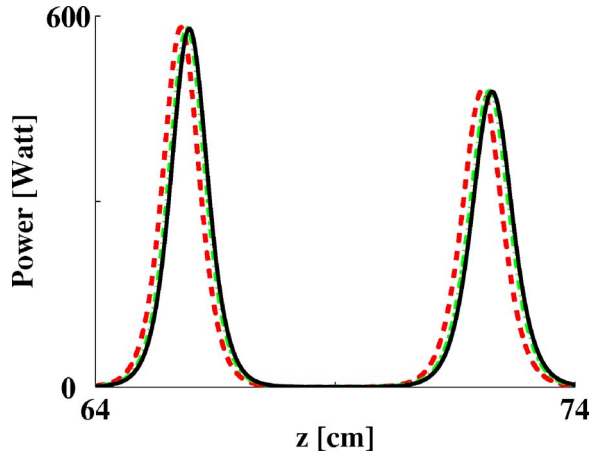

Fig. 6. (Color online) Intensity of the two solitons after their interaction calculated at $t = 25.52$ ns. The spatial step size was equal to $\Delta Z = W_S/40$ and the temporal step size was equal to $\Delta T = W_S/(8000V_g)$ (solid curve), $\Delta T = W_S/(1600V_g)$ (dashed–dotted curve), and $\Delta T = W_S/(800V_g)$ (dashed curve).

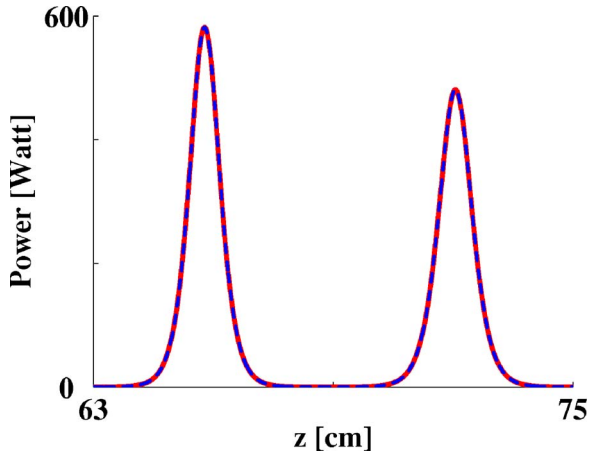

Fig. 8. (Color online) Intensity of two solitons after their interaction, calculated at $t = 25.52$ ns using nonsymmetrized OSSM for a spatial step size of $\Delta Z = W_S/800$ (solid curve) and $\Delta Z = W_S/80$ (dashed curve). The temporal step size was equal to $\Delta T = W_S/(800V_g)$ in both cases.

cation of the ith soliton at $t=t_1$, and $Z_i(t_2)$ is the location of ith soliton at $t=t_2$. The spatial step size was equal to $\Delta Z=W_s/40$. Using a temporal step size $\Delta T=W_s/800V_g$ the speed of the first soliton ($i=1$) was equal to $0.1196V_g$ and the speed of the second soliton was equal to $0.0997Vg$. Using a temporal step size $\Delta T=W_s/1600V_g$, the speeds of the two solitons were $0.1199V_g$ and $0.0999V_g$. Using a temporal step size of $\Delta T=W_s/8000V_g$, the speeds of the two solitons were equal to $0.12V_g$ and $0.0999V_g$. Therefore, as obtained in the simulation of a single soliton, the error in the solitons' velocity is very small.

We compared the results after the interaction at $t=25.52$ ns using different widths of the window function. The temporal and the spatial step sizes were equal to $\Delta T=W_s/1600V_g$ and $\Delta Z=W_s/40$, respectively. The widths of the window function were changed between 105 to 155 cm. The width of the absorbing layer was equal to $L_a=5$ cm. The solution for different window widths was compared to that obtained using a window of 155 cm. The relative errors obtained for window widths of $L=135$, 125, 115, and 105 cm were equal to $\varepsilon=0.0033\%$, 0.0038%, 0.0034%, and 0.0053%, respectively. Therefore, a window with a length of $L=105$ cm, as used in Figs. 5–8, is sufficient for obtaining an accurate result.

C. Bistability

In the next example we use the nonsymmetrized OSSM for analyzing a device with bistable behavior. The analyzed device had the same parameters as given in [3]. The grating had a length of $L=1$ m, a nonlinear coefficient of $\Gamma=0.1$ m^{-1} W^{-1}, and a coupling coefficient of $\kappa=5$ m^{-1}. The input wave was a continuous-wave signal with a detuning parameter that was equal to $\delta=4.75$ m^{-1}. The boundary conditions were equal to $u_-(z=L,t)=0$, $u_+(z=0,t)=A$. The solution was first calculated for an amplitude A that was increased between 0 to 2 $\sqrt{\text{W}}$ in steps of 0.01 $\sqrt{\text{W}}$. Then, the solution was calculated again for an amplitude A that was decreased to 0 in steps of 0.01 $\sqrt{\text{W}}$.

Figure 9 shows the device transmissivity as a function of the incoming amplitude. The device was analyzed using a spatial step size $\Delta Z=0.002$ m (solid curve) and $\Delta Z=0.008$ m (dashed curve). The temporal step size was equal to $\Delta T=0.002/V_g$ s. The figure shows that the increase in the spatial step size ΔZ did not add a significant error. The relative error between the two results was equal to 1%. However, the increase in the spatial step size by a factor of 4 enabled the reduction of run time from 18 to 6.4 h. We note that in [3] a similar bistable curve was obtained using a direct numerical integration of the NLCME.

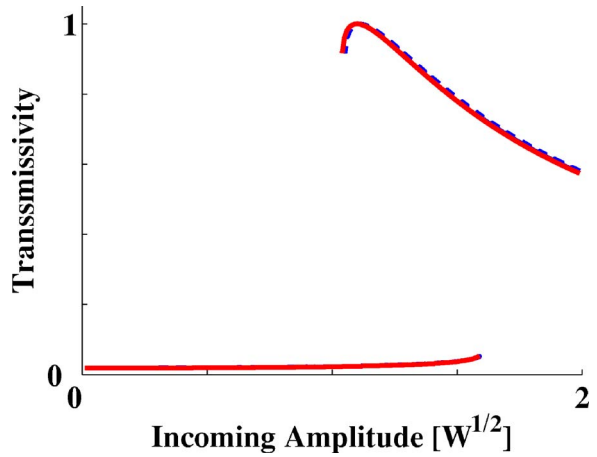

Fig. 9. (Color online) Transmissivity versus the incoming amplitude of a bistable device formed by a uniform FBG.

D. Launching of a Soliton

In the last example, we use the nonsymmetrized OSSM for analyzing the launching of a gap soliton. The grating consists of an apodization region that is used to efficiently launch the soliton in a uniform region where the soliton propagates. The apodization segment had a quarter-period sine profile with a length $L_1=2$ cm. The uniform grating section had a length $L_2=26$ cm and an amplitude $\kappa=9000$ m^{-1}. The nonlinear coefficient was equal to $\Gamma=5$ W^{-1} km^{-1}, and the effective refractive index in the absence of the grating was equal to $n=1.45$. The boundary condition was $u_+(z=0,t)=\sqrt{34}\,\text{sech}[(t-3T_0)/0.5499T_0]$, where $T_0=640$ ps. The incident pulse had a spatial FWHM of 13.24 cm, a peak power of 34 W, and a detuning parameter that was equal to $\delta=9031$ m^{-1}. In this example, the grating is half infinite and the parameters of the window function were chosen as follows: $L=40$ cm, $L_w=30$ cm, and $L_a=2$ cm. The spatial and the temporal step sizes in the apodized region were equal to $\Delta Z=0.005$ mm and $\Delta T=0.005$ mm$/V_g$ s, respectively.

In the uniform region, the spatial and the temporal step size were equal to $\Delta Z=1$ mm and $\Delta T=0.005$ mm$/V_g$ s, respectively. We have started the simulation with a spatial and a temporal step size of $\Delta Z=0.005$ mm and $\Delta T=0.005$ mm$/V_g$ s, respectively. To increase the spatial step size ΔZ in the uniform region of the grating, we have tracked the location of the signal peak along the propagation. When the location of the peak intensity was 30 mm inside the uniform grating section, the spatial step size was increased to 1 mm and the

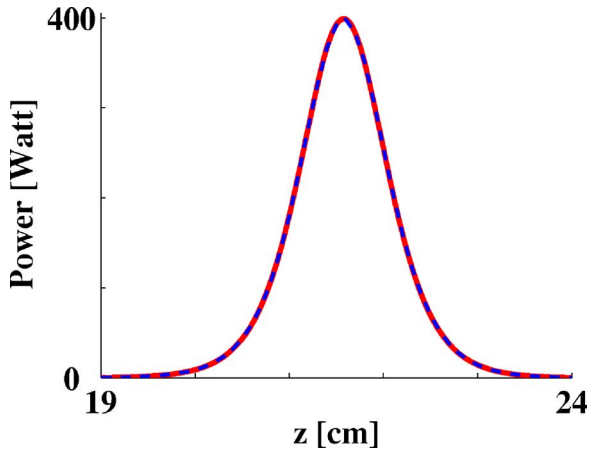

Fig. 10. (Color online) Output intensity after launching an input hyperbolic-secant pulse through an apodization section and 19 cm of uniform grating. The solid curve gives the result calculated using a uniform spatial step size with $\Delta Z=V_g\Delta T=0.005$ mm, and the dashed curve gives the result obtained using nonsymmetrized OSSM with a nonuniform spatial step size with $\Delta Z=V_g\Delta T=0.005$ mm in the apodized grating region and $\Delta Z=1$ mm, $V_g\Delta T=0.005$ mm in the uniform region.

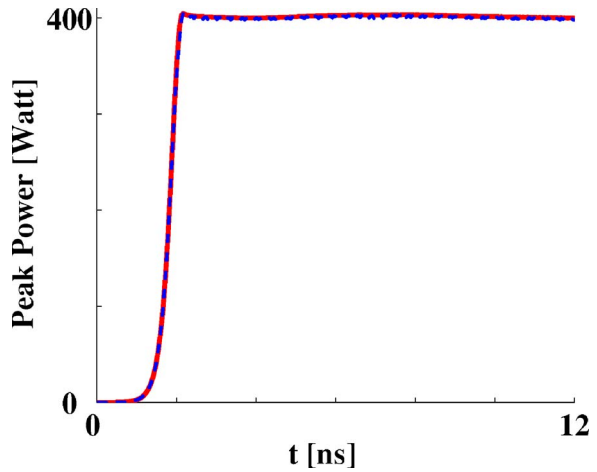

Fig. 11. (Color online) Peak power as a function of the propagation duration obtained by using a uniform spatial step size (solid curve) and by using nonsymmetrized OSSM with a nonuniform spatial step size (dashed curve). The simulation parameters are the same as used in Fig. 10.

temporal step size was kept constant, $\Delta T = 0.005\ \mathrm{mm}/V_g\ \mathrm{s}$. The results were compared to those obtained using constant spatial and temporal step sizes of $\Delta Z = 0.005\ \mathrm{mm}$ and $\Delta T = 0.005\ \mathrm{mm}/V_g\ \mathrm{s}$, respectively, as used in [14]. Figure 10 shows a comparison between the pulse intensities at $t = 12.91\ \mathrm{ns}$, which corresponds to a propagation of 19 cm in the uniform grating region. Figure 11 compares the peak intensity as a function of time of the two solutions. The relative error in the peak intensity at $t = 12.91\ \mathrm{ns}$ between the solution with the uniform spatial step size and the solution with the varying spatial step size was equal to $\epsilon_a = 0.1\%$.

The control of the spatial resolution along the grating made it possible to decrease the run time from 604 to 178 min. In the uniform grating section, the run time was decreased by a factor of ~100 from 393 to 4 min. The spatial step size could be significantly increased inside the uniform grating section without affecting the error, since the change in the pulse shape in that region is slow. In the apodization section, the input pulse significantly changes until it becomes a soliton, and therefore the spatial step size should be kept small.

We would like to note that the first, the second, and the last examples given in this section run on an X4100 AMD 64× processor with 8 Gbytes of memory. The third example runs on a PC-Pentium IV with a 1.8 GHz dual-core processor and 1 Gbyte of memory. All the examples were implemented using MATLAB software.

4. CONCLUSION

In conclusion, we have demonstrated and studied the performance of an optimized split-step method (OSSM) for solving the nonlinear coupled-mode equations that are used to model nonlinear pulse propagation in FBGs. We have used the method to numerically analyze a single soliton propagation, two solitons' interaction, bistable behavior, and a soliton launching in FBGs. Unlike in the numerical methods that were previously demonstrated, the OSSM does not require a direct connection between the temporal and the spatial step size. Therefore, the spatial step size may be significantly increased without affecting the accuracy of the result. Hence, we could decrease in some problems the run time by a factor of up to 100. To implement the method, a generalized solution for solving the nonlinear operator in the split-step procedure was developed. We have found that the use of nonsymmetrized OSSM is enough to obtain accurate results with a short run time. The spatial step size can be dynamically controlled along the grating. The maximum spatial step size is obtained in grating regions where the change in the propagating pulses is relatively slow, as occurred, for example, during a soliton propagation. When analyzing the propagation of a pulse using nonsymmetrized OSSM, the main error is obtained in the location of the propagating pulse and not in the pulse amplitude. Since a small shift in the pulse location usually does not have a significant physical meaning, one may increase the temporal step size and ignore the very small error in the pulse speed. The Richardson extrapolation was used to slightly decrease the run time.

ACKNOWLEDGMENT

This work was supported by the Israel Science Foundation (ISF) of the Israeli Academy of Sciences.

REFERENCES

1. H. G. Winful, "Pulse compression in optical fiber filters," Appl. Phys. Lett. **46**, 527–529 (1985).
2. A. Rosenthal and M. Horowitz, "Bragg-soliton formation and pulse compression in a one-dimensional periodic structure," Phys. Rev. E **74**, 066611 (2006).
3. C. M. de Sterke and J. E. Sipe, "Switching dynamics of finite periodic nonlinear media: a numerical study," Phys. Rev. A **42**, 2858–2869 (1990).
4. S. Pereira and J. E. Sipe, "Nonlinear pulse propagation in birefringent fiber Bragg gratings," Opt. Express **3**, 418–432 (1998).
5. D. Taverner, N. G. R. Broderick, D. J. Richardson, M. Ibsen, and R. I. Laming, "All-optical AND gate based on coupled gap-soliton formation in a fiber Bragg grating," Opt. Lett. **23**, 259–261 (1998).
6. Y. P. Shapira and M. Horowitz, "Optical AND gate based on soliton interaction in a fiber Bragg grating," Opt. Lett. **32**, 1211–1213 (2007).
7. J. T. Mok, C. M. de Sterke, I. C. M. Littler, and B. J. Eggleton, "Dispersionless slow light using gap solitons," Nat. Phys. **2**, 775–780 (2006).
8. J. T. Mok, C. M. de Sterke, and B. J. Eggleton, "Delay-tunable gap soliton-based slow-light system," Opt. Express **14**, 11987–11996 (2006).
9. A. B. Aceves and S. Wabnitz, "Self-induced transparency solitons in nonlinear refractive periodic media," Phys. Lett. A **141**, 37–42 (1989).
10. D. N. Christodoulides and R. I. Joseph, "Slow Bragg solitons in nonlinear periodic structures," Phys. Rev. Lett. **62**, 1746–1749 (1989).
11. C. M. de Sterke and J. E. Sipe, "Gap solitons," in *Progress in Optics XXXIII*, E. Wolf, ed. (Elsevier, 1994), pp. 203–260.
12. W. C. K. Mak, B. A. Malomed, and P. L. Chu, "Formation of a standing light pulse through collision of gap solitons," Phys. Rev. E **68**, 26609 (2003).
13. C. M. de Sterke, K. R. Jackson, and B. D. Robert, "Nonlinear coupled-mode equations on a finite interval: a numerical procedure," J. Opt. Soc. Am. B **8**, 403–412 (1991).
14. A. Rosenthal and M. Horowitz, "Analysis and design of

nonlinear fiber Bragg gratings and their application for optical compression of reflected pulses," Opt. Lett. **31**, 1334–1336 (2006).
15. O. V. Sinkin, J. Zweck, and C. R. Menyuk, "Optimization of the split-step Fourier method in modeling optical-fiber communications systems," J. Lightwave Technol. **21**, 61–68 (2003).
16. R. L. Burden and J. D. Faires, "Richardson's extrapolation," in *Numerical Analysis* (ITP, 1997), pp. 180–183.
17. G. P. Agrawal, "Numerical methods," in *Nonlinear Fiber Optics* (Academic, 1995), pp. 50–55.
18. C. E. Shannon, "Communication in the presence of noise," Proc. IRE **37**, 10–21 (1949).
19. J. Saijonmaa and D. Yevick, "Beam-propagation analysis of loss in bent optical waveguides and fibers," J. Opt. Soc. Am. **73**, 1785–1791 (1983).
20. M. D. Feit and J. A. Fleck, Jr., "Light propagation in graded-index optical fibers," Appl. Opt. **17**, 3990–3998 (1978).
21. C. Vassallo and F. Collino, "Highly efficient absorbing boundary conditions for the beam propagation method," J. Lightwave Technol. **14**, 1570–1577 (1996).
22. J. P. Berenger, "A perfectly matched layer for the absorption of electromagnetic waves," J. Comput. Phys. **114**, 185–200 (1994).
23. T. Dohnal and T. Hagstrom, "Perfectly matched layers in photonics computations: 1D and 2D nonlinear coupled mode equations," J. Comput. Phys. **223**, 690–710 (2007).